TECHNICAL NOTE

D-788

SUBSONIC LONGITUDINAL AERODYNAMIC CHARACTERISTICS OF DISKS WITH ELLIPTIC CROSS SECTIONS AND THICKNESS-DIAMETER RATIOS FROM 0.225 TO 0.425

By Fred A. Demele and Jack J. Brownson

Ames Research Center
Moffett Field, Calif.

NATIONAL AERONAUTICS AND SPACE ADMINISTRATION

WASHINGTON

April 1961

590322
26p.

NATIONAL AERONAUTICS AND SPACE ADMINISTRATION

TECHNICAL NOTE D-788

SUBSONIC LONGITUDINAL AERODYNAMIC CHARACTERISTICS OF DISKS WITH ELLIPTIC CROSS SECTIONS AND THICKNESS-DIAMETER RATIOS FROM 0.225 TO 0.425

By Fred A. Demele and Jack J. Brownson

SUMMARY

An investigation has been made to determine the effects of thickness on the longitudinal aerodynamic characteristics of a family of disk-shaped bodies which might find application in the design of re-entry vehicles. The models had elliptic profiles which varied in maximum thickness from 0.225 to 0.425 diameter. The tests were conducted to maximum angles of attack of 25° over a range of Mach numbers from 0.25 to 0.90 at a Reynolds number of 3.3×10^6 and at Reynolds numbers to 16×10^6 at a Mach number of 0.25.

It was found that with the moment center located at 40 percent of the diameter, the models were longitudinally unstable throughout the subsonic speed range. Increasing the thickness resulted in greater instability at low speeds but had little effect at high subsonic speeds. Increasing the Reynolds number from 3.3×10^6 to 16×10^6 resulted in large reductions in longitudinal instability and generally increased the lift-curve slope. Large increases in drag at lifting conditions accompanied increases in thickness. At low speeds the peak value of maximum lift-drag ratio, which was about 8 for a thickness-diameter ratio of 0.225, decreased to 4 as a result of increasing thickness-diameter ratio to 0.425.

INTRODUCTION

General interest in manned space flight has provided a stimulus for the investigation of shapes which appear to be attractive for application to re-entry vehicles. Such vehicles can be classed as either nonlifting or lifting. Nonlifting types, such as used in Project Mercury, have certain advantages which include structural simplicity, no requirement for an elaborate flight-control system, ease of mating with the booster, and short exposure times to high heating rates during entry. Advantages of lifting types, by comparison, include lower peak heating rates and

decelerations, the possibility for a conventional horizontal landing, and the ability to maneuver, thus providing control over longitudinal and lateral range and a wider entry corridor on return from planetary or lunar missions (see, e.g., ref. 1).

A lifting shape which appears attractive in terms of the foregoing considerations is a thick disk. At high attitudes, the weight to drag ratio is low and the radius of curvature of the surface exposed to the airstream is large, a combination of parameters which results in reduced convective heating rates (see, e.g., ref. 2). The low-speed lift-drag ratios associated with this type of shape (see, e.g., ref. 3) appear sufficiently high to permit a conventional horizontal landing.

The investigation reported herein was undertaken to assess the effects of thickness on the aerodynamic characteristics of disk shapes suitable for lifting re-entry into the earth's atmosphere and potentially capable of conventional horizontal landing. The models had elliptic cross sections which varied in thickness from 0.225 to 0.425 diameter. The tests were conducted in the Ames 12-Foot Pressure Wind Tunnel over a Mach number range from 0.25 to 0.90 at a Reynolds number of 3.3×10^6 and at Reynolds numbers to 16×10^6 at a Mach number of 0.25. Tests on similar shapes have been conducted at subsonic, transonic, and supersonic speeds and the results have been presented in references 4, 5, and 6.

NOTATION

A surface area

C_D drag coefficient, $\frac{\text{drag}}{qS}$

C_L lift coefficient, $\frac{\text{lift}}{qS}$

C_m pitching-moment coefficient, $\frac{\text{pitching moment}}{qSd}$, referred to 40 percent of model diameter on the chord plane

d diameter of model

$\frac{L}{D}$ lift-drag ratio

M free-stream Mach number

q free-stream dynamic pressure

R Reynolds number, based on the model diameter

r radial distance from center of model

S	plan-form area of model
$\frac{t}{d}$	maximum thickness to diameter ratio
V	volume
y	vertical distance from the chord plane
α	angle of attack, measured with respect ot the chord plane
$\frac{dC_L}{d\alpha}$	lift-curve slope in the vicinity of $\alpha = 0^\circ$ to 5°
$\frac{dC_m}{dC_L}$	pitching-moment-curve slope in the vicinity of $C_L = 0$ to 0.1

Subscripts

D	disk
max	maximum
S	sphere
0	zero lift

MODELS

Four smoothly finished wooden models having diameters of 2 feet and maximum thickness-diameter ratios of 0.225, 0.325, 0.375, and 0.425 were used for the investigation. All models had elliptical thickness distributions; however, those with thickness-diameter ratios of 0.325 and 0.425 were symmetric, whereas those with thickness-diameter ratios of 0.225 and 0.375 incorporated a 2.5-percent semielliptic mean line camber. The disk shapes were generated by revolving about the minor axis the elliptic sections defined by the coordinates given in table I. The corresponding volumes and surface areas of the resultant shapes relative to those of a sphere are given in table II.

The models were sting supported as shown in figure 1. A six-component strain-gage balance enclosed in the models measured the forces and moments. A cylindrical fairing was provided at the base of the models to enclose the sting within the body (see fig. 1). Base pressures were obtained from an orifice located just inside the base of the sting fairing.

TESTS

Longitudinal force and moment data were obtained throughout an angle-of-attack range from -3° to 25°. The investigation was made over a Mach number range of 0.25 to 0.90 at a Reynolds number of 3.3×10^{6}, and over a Reynolds number range of 3.3×10^{6} to 16×10^{6} at a Mach number of 0.25. Results were obtained for symmetrical profiles with thickness-diameter ratios of 0.425 and 0.325 and for 2.5-percent positive- and negative-camber profiles with thickness-diameter ratios of 0.375 and 0.225. The tests were conducted with the models in a clean condition, that is, without boundary-layer transition-fixing devices.

CORRECTIONS TO DATA

The data have been corrected by the method of reference 7 for wind-tunnel-wall interference associated with lift on the model. The magnitudes of the corrections which were added to the measured values are as follows:

$$\Delta\alpha = 0.21\ C_L$$

$$\Delta C_D = 0.0036\ C_L^{2}$$

Corrections to the data to account for the effects of constriction due to the wind-tunnel walls were calculated by the method of reference 8. At a Mach number of 0.90, the correction amounted to an increase of about 1.5 percent in the measured value of Mach number and dynamic pressure.

The drag data have been adjusted to correspond to a base pressure equal to free-stream static pressure. The area of the base of the sting fairing, 0.041 square feet, was used for this correction.

RESULTS AND DISCUSSION

The basic longitudinal characteristics are presented in figure 2 for Reynolds numbers of 3.3×10^{6} and 16×10^{6} at a Mach number of 0.25 and in figure 3 for Mach numbers from 0.60 to 0.90 at a Reynolds number of 3.3×10^{6}. A comparison of the effects of positive and negative camber on selected characteristics is shown in figures 4 and 5. Figures 6 and 7 summarize the effects of varying thickness on selected longitudinal characteristics. The lift-curve slopes presented in figures 5 and 7 represent average values between angles of attack of 0° and 5°. Because of the nonlinearity of the pitching-moment curves, the slopes presented

in figures 5 and 7 were arbitrarily taken between lift coefficients of 0 and 0.1 and are only indicative of the longitudinal stability at low lift coefficients.

The data in figures 2 and 3 show that with the moment center located at 40 percent of the diameter, the models were unstable throughout the angle-of-attack range of the investigation. Increasing Reynolds number from 3.3×10^6 to 16×10^6 at low speeds reduced this instability considerably as shown in figures 2, 5, and 7. It is also evident that in most cases increasing Reynolds number resulted in increased lift-curve slopes. Further, it is shown in figure 2 that although the maximum lift-drag ratio did not necessarily increase as a result of a change in Reynolds numbers from 3.3×10^6 to 16×10^6, the lift-drag ratio almost always improved at lift coefficients higher than those for maximum lift-drag ratio.

The curves in figure 4 indicate only small differences in drag between positive and negative camber except at lifting conditions in the region of drag divergence for the model having a thickness-diameter ratio of 0.375. Likewise, as shown in figure 5, camber generally caused only small differences in maximum lift-drag ratio and the lift coefficient at which it occurred. However, larger differences were evidenced in lift- and pitching-moment-curve slopes (fig. 5), although these differences were inconsistent between models having a thickness-diameter ratio of 0.225 and those having a thickness-diameter ratio of 0.375.

The effects of thickness on drag are summarized in figure 6 and on maximum lift-drag ratio, and lift- and pitching-moment-curve slopes in figure 7. Since data were not obtained for models with zero camber at thickness ratios of 0.225 and 0.375, averaged values for positive and negative camber were used for the summary curves. As shown in figure 6, large increases in drag accompanied increases in thickness at all lifting conditions, particularly at high subsonic speeds. Correspondingly, maximum lift-drag ratio, which at low speeds had a peak value of about 8 for a thickness-diameter ratio of 0.225 (fig. 7), decreased to 4 as a result of increasing the thickness ratio to 0.425. Larger reductions in maximum lift-drag ratio resulted from increasing thickness at high subsonic speeds, primarily because of large increases in minimum drag coefficient. Increasing thickness also resulted in reductions in lift-curve slope (fig. 7). At low speeds, the longitudinal instability noted earlier became more severe with increasing thickness. However, at a Mach number of 0.85, thickness appeared to have little effect on the stability.

Ames Research Center
National Aeronautics and Space Administration
Moffett Field, Calif., Jan. 19, 1961

REFERENCES

1. Chapman, Dean R.: An Analysis of the Corridor and Guidance Requirements for Supercircular Entry Into Planetary Atmospheres. NASA TR R-55, 1960.

2. Chapman, Dean R.: An Approximate Analytical Method for Studying Entry Into Planetary Atmospheres. NASA TR R-11, 1959. (Supersedes NACA TN 4276)

3. Zimmerman, C. H.: Aerodynamic Characteristics of Several Airfoils of Low Aspect Ratio. NACA TN 539, 1935.

4. Ware, George M.: Static Stability and Control Characteristics at Low-Subsonic Speeds of a Lenticular Reentry Configuration. NASA TM X-431, 1960.

5. Mugler, John P., Jr., and Olstad, Walter B.: Static Longitudinal Aerodynamic Characteristics at Transonic Speeds of a Lenticular-Shaped Reentry Vehicle. NASA TM X-423, 1960.

6. Jackson, Charlie M., Jr., and Harris, Roy V., Jr.: Static Longitudinal Stability and Control Characteristics at a Mach Number of 1.99 of a Lenticular-Shaped Reentry Vehicle. NASA TN D-514, 1960.

7. Glauert, H.: The Elements of Airfoils and Airscrew Theory. American Ed., The Macmillan Company, N. Y., 1943, p. 191.

8. Herriot, John G.: Blockage Corrections for Three-Dimensional-Flow Closed Throat Wind Tunnels, With Consideration of the Effect of Compressibility. NACA Rep. 995, 1950. (Supersedes NACA RM A7B28)

TABLE I.- COORDINATES OF SURFACE OF MODELS
[All dimensions in inches]

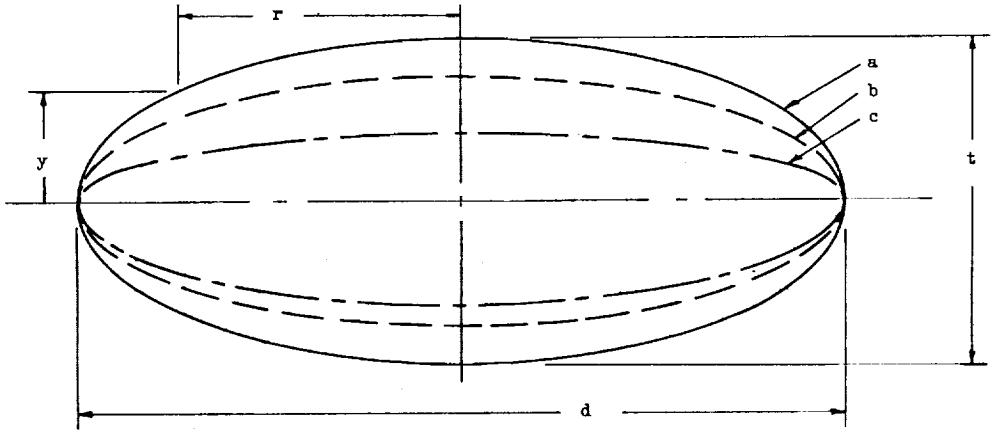

r	t/d=.425	0.375		0.325	0.225	
	$\pm y_a$	$+ y_b$	$- y_a$	$\pm y_b$	$+ y_c$	$- y_c$
0	5.10	3.90	5.10	3.90	2.10	3.30
1.00	5.08	3.89	5.08	3.89	2.09	3.29
2.00	5.03	3.84	5.03	3.84	2.07	3.25
3.00	4.94	3.78	4.94	3.78	2.03	3.20
4.00	4.81	3.68	4.81	3.68	1.98	3.11
5.00	4.64	3.54	4.64	3.54	1.91	3.00
6.00	4.42	3.38	4.42	3.38	1.82	2.86
7.00	4.14	3.17	4.14	3.17	1.71	2.68
7.50	3.98	3.04	3.98	3.04	1.64	2.58
8.00	3.80	2.91	3.80	2.91	1.56	2.46
8.50	3.60	2.75	3.60	2.75	1.48	2.33
9.00	3.37	2.58	3.37	2.58	1.39	2.18
9.50	3.12	2.38	3.12	2.38	1.28	2.02
10.00	2.82	2.16	2.82	2.16	1.16	1.82
10.50	2.47	1.89	2.47	1.89	1.02	1.60
10.75	2.27	1.73	2.27	1.73	.93	1.47
11.00	2.04	1.56	2.04	1.56	.84	1.32
11.25	1.78	1.36	1.78	1.36	.73	1.15
11.50	1.46	1.11	1.46	1.11	.60	.94
11.60	1.31	1.00	1.31	1.00	.54	.84
11.70	1.13	.87	1.13	.87	.47	.73
11.80	.93	.71	.93	.71	.38	.60
11.90	.66	.50	.66	.50	.27	.42
11.95	.46	.36	.46	.36	.19	.30
12.00	0	0	0	0	0	0

TABLE II.- VOLUME AND SURFACE AREA OF ELLIPTIC DISKS

RELATIVE TO SPHERE

$\frac{V_D}{V_S} = \frac{t}{d}$	$\frac{A_D}{A_S}$	$\frac{(V/A)_D}{(V/A)_S}$
0.225	0.556	0.405
.325	.600	.542
.375	.624	.600
.425	.650	.654

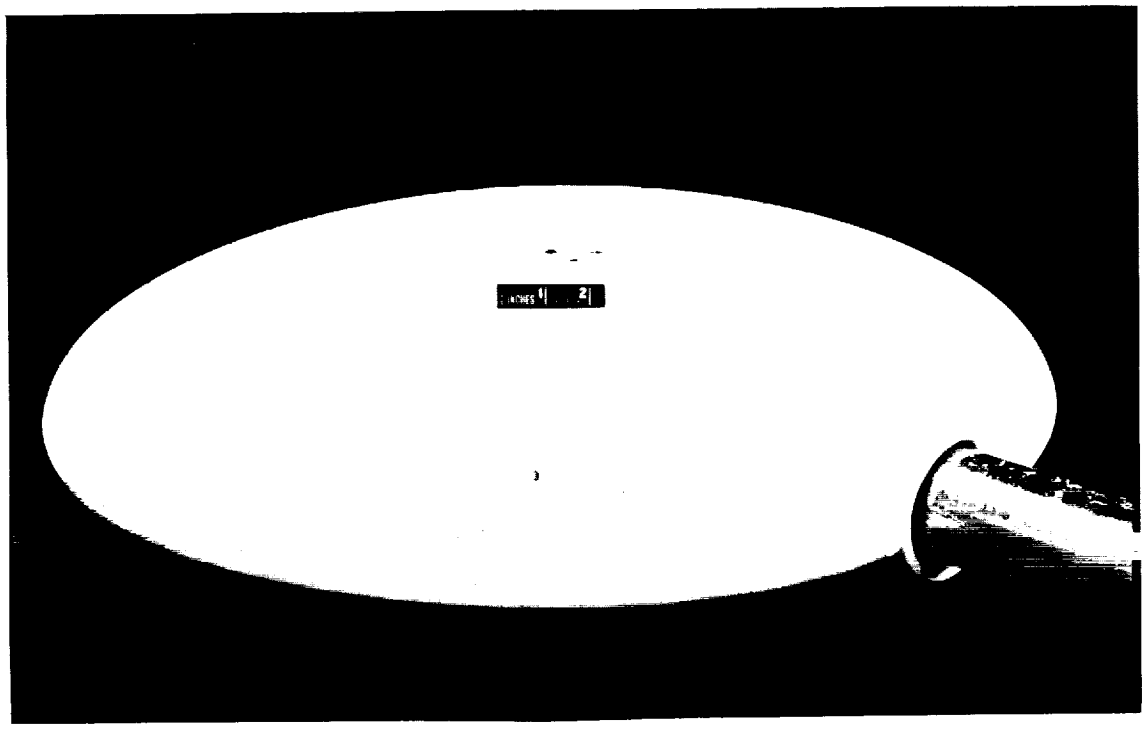

(a) t/d = 0.225

A-26180

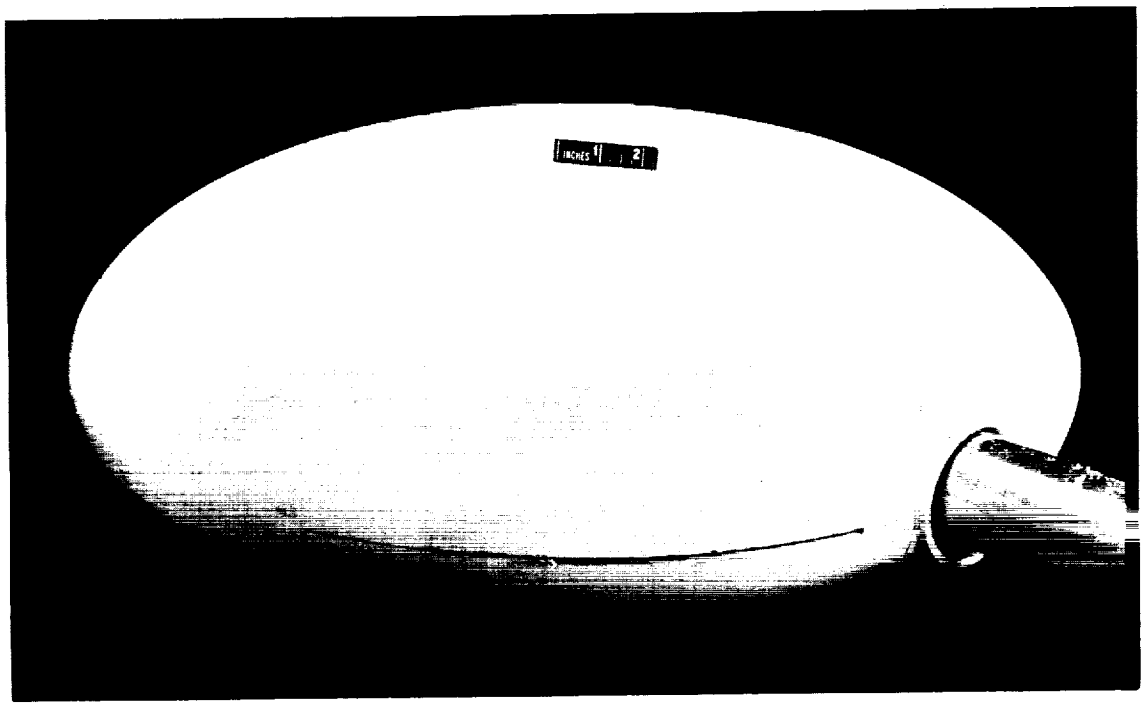

(b) t/d = 0.425

A-26183

Figure 1.- Photographs of two models.

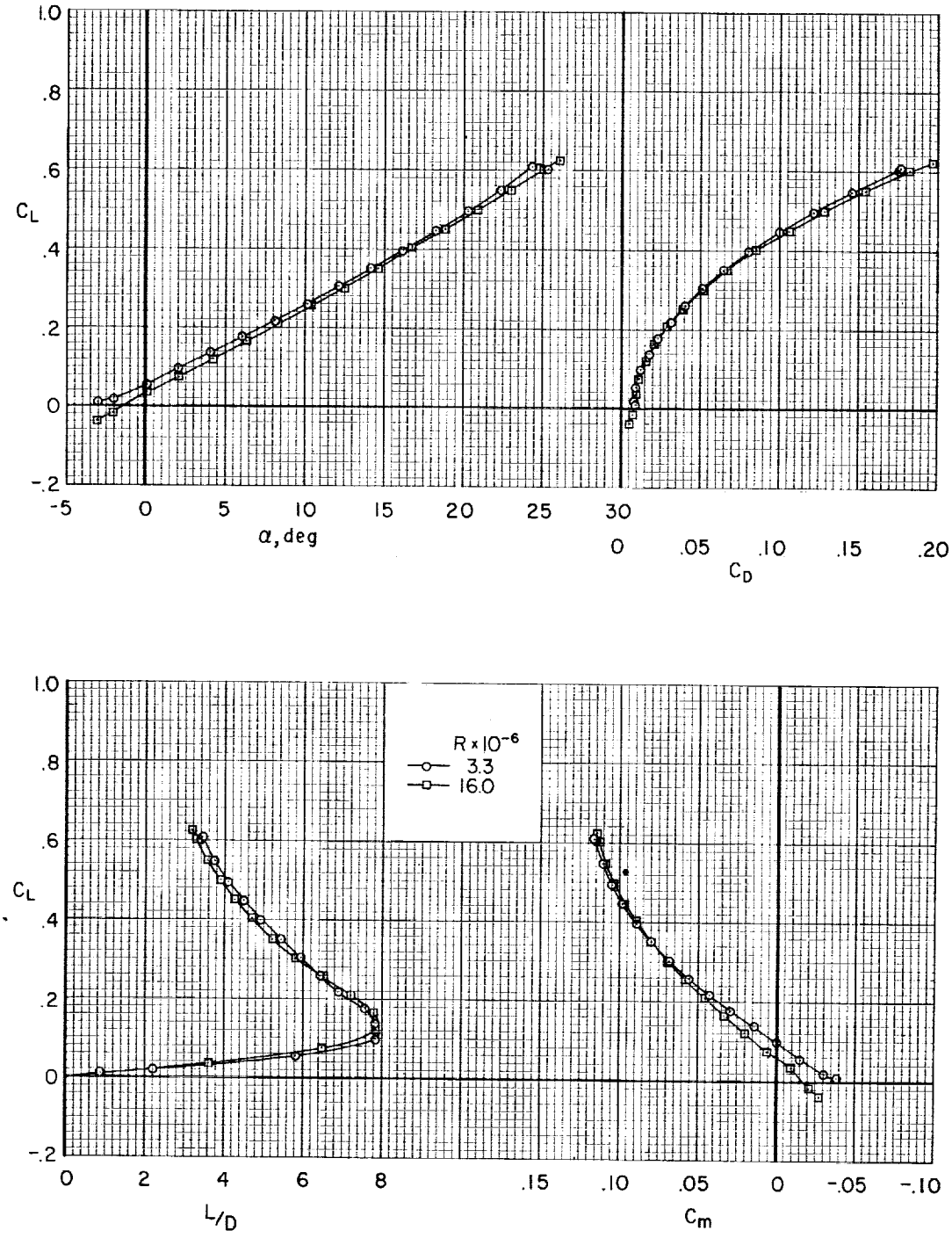

(a) t/d = 0.225, positive camber.

Figure 2.- The longitudinal aerodynamic characteristics of the models at Reynolds numbers of 3.3×10^6 and 16×10^6; M = 0.25.

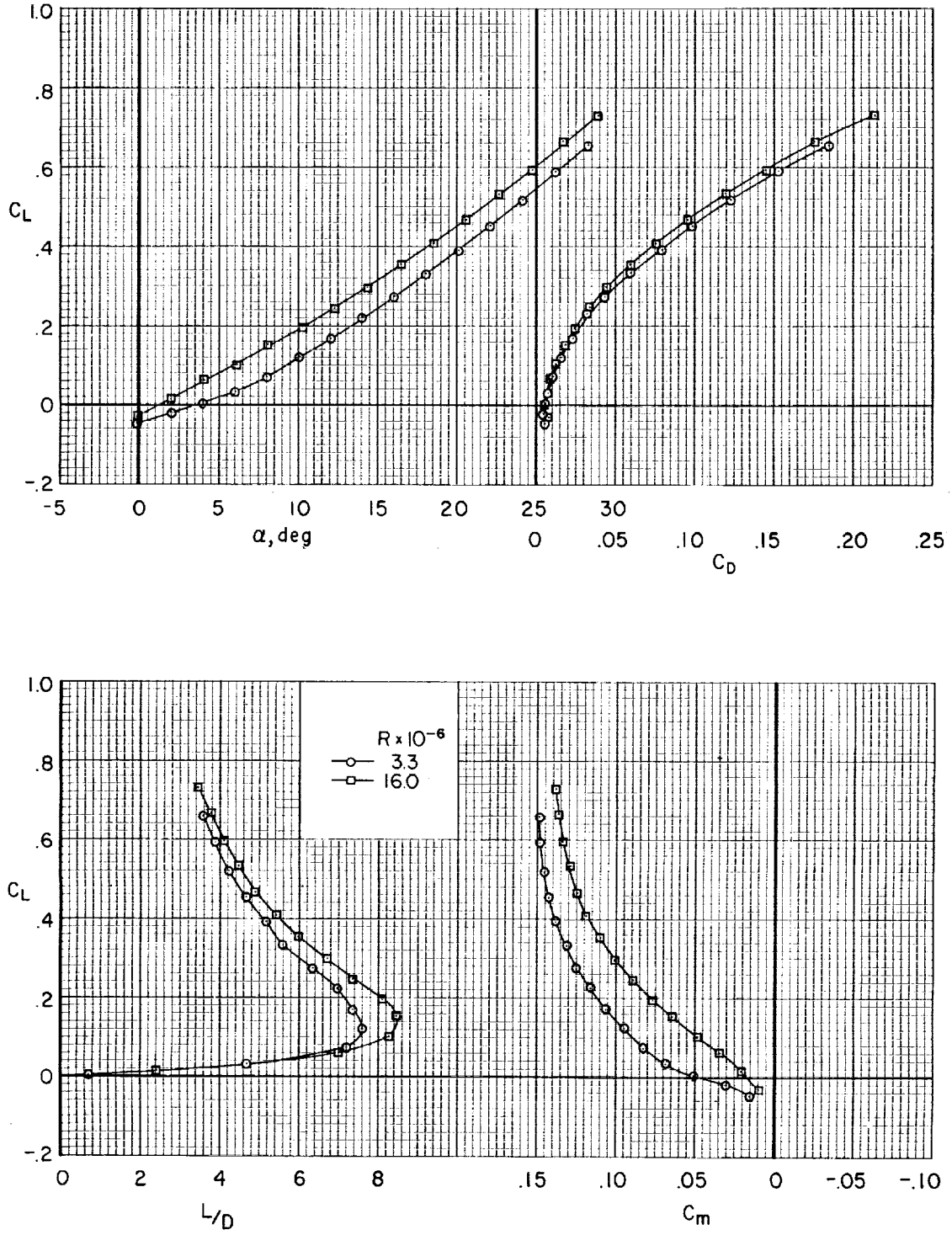

(b) t/d = 0.225, negative camber.

Figure 2.- Continued.

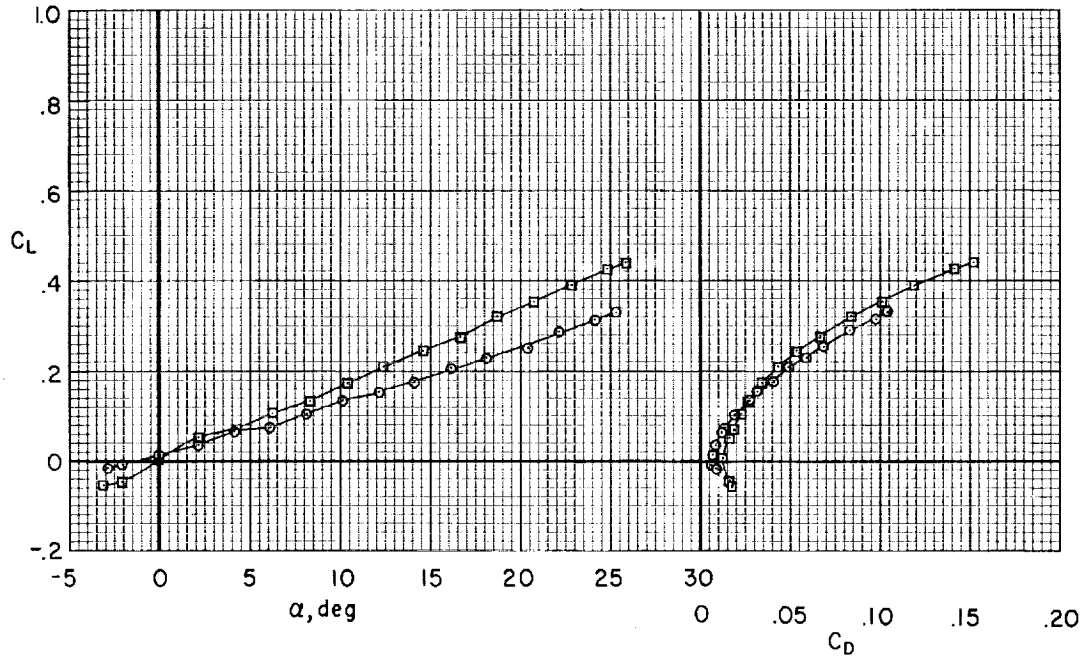

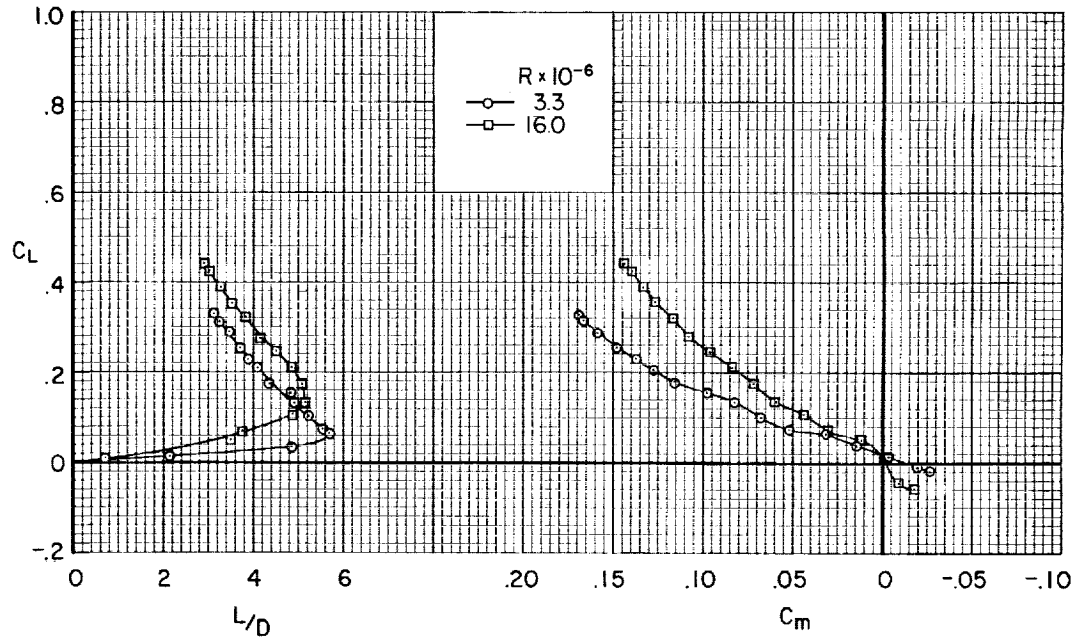

(c) t/d = 0.325

Figure 2.- Continued.

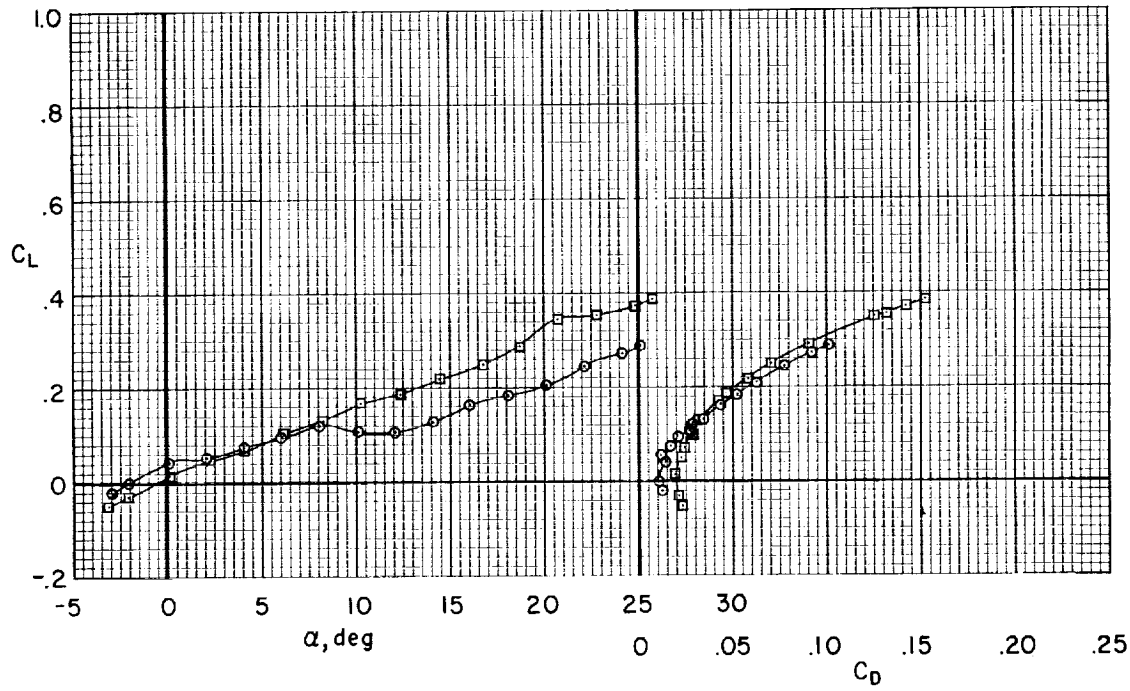

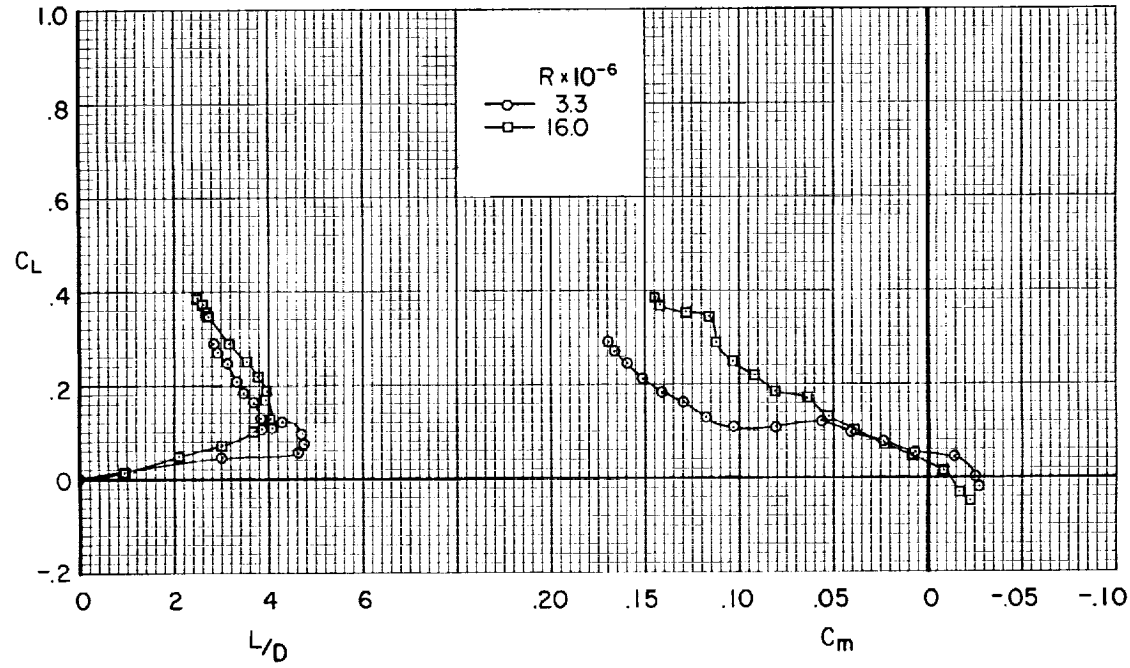

(d) t/d = 0.375, positive camber.

Figure 2.- Continued.

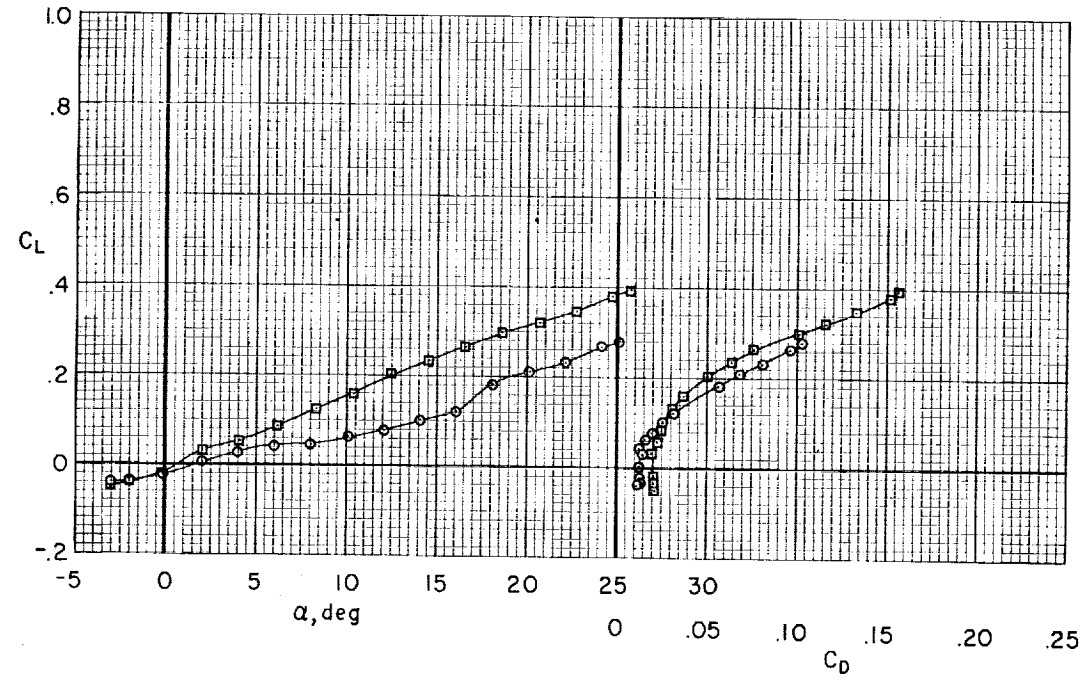

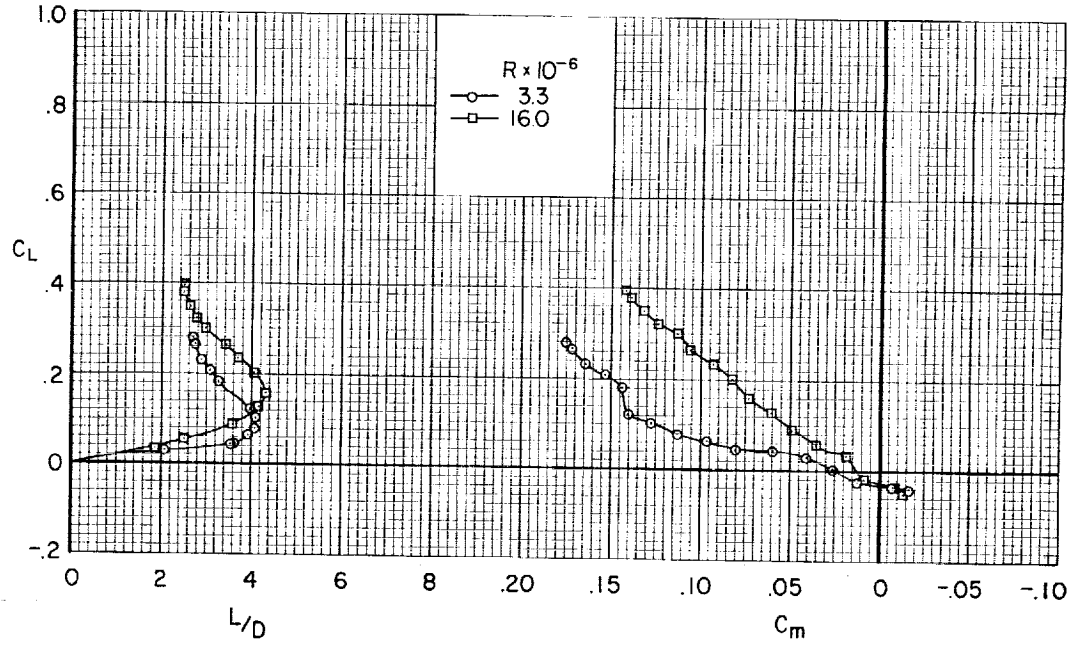

(e) t/d = 0.375, negative camber.

Figure 2.- Continued.

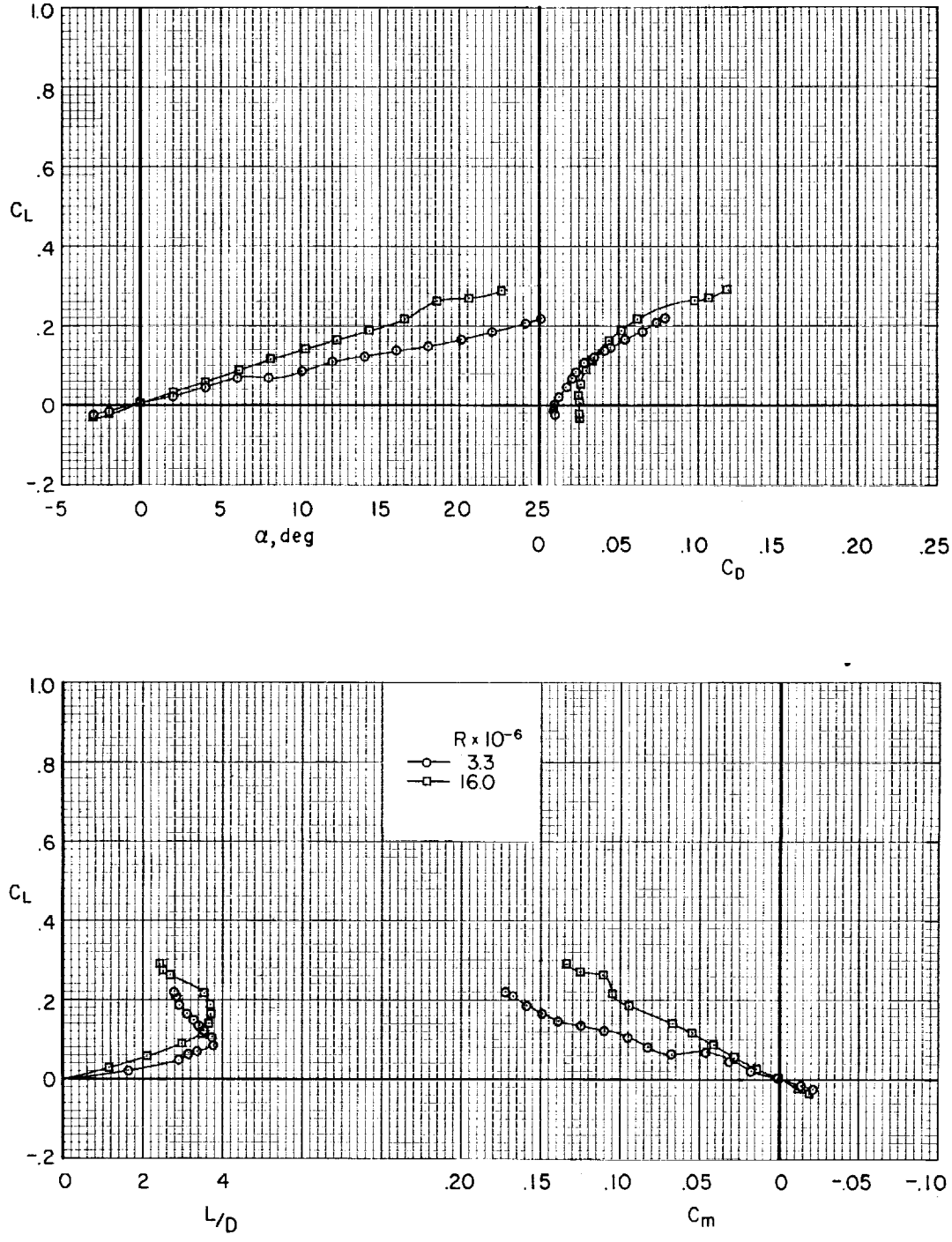

(f) t/d = 0.425

Figure 2.- Concluded.

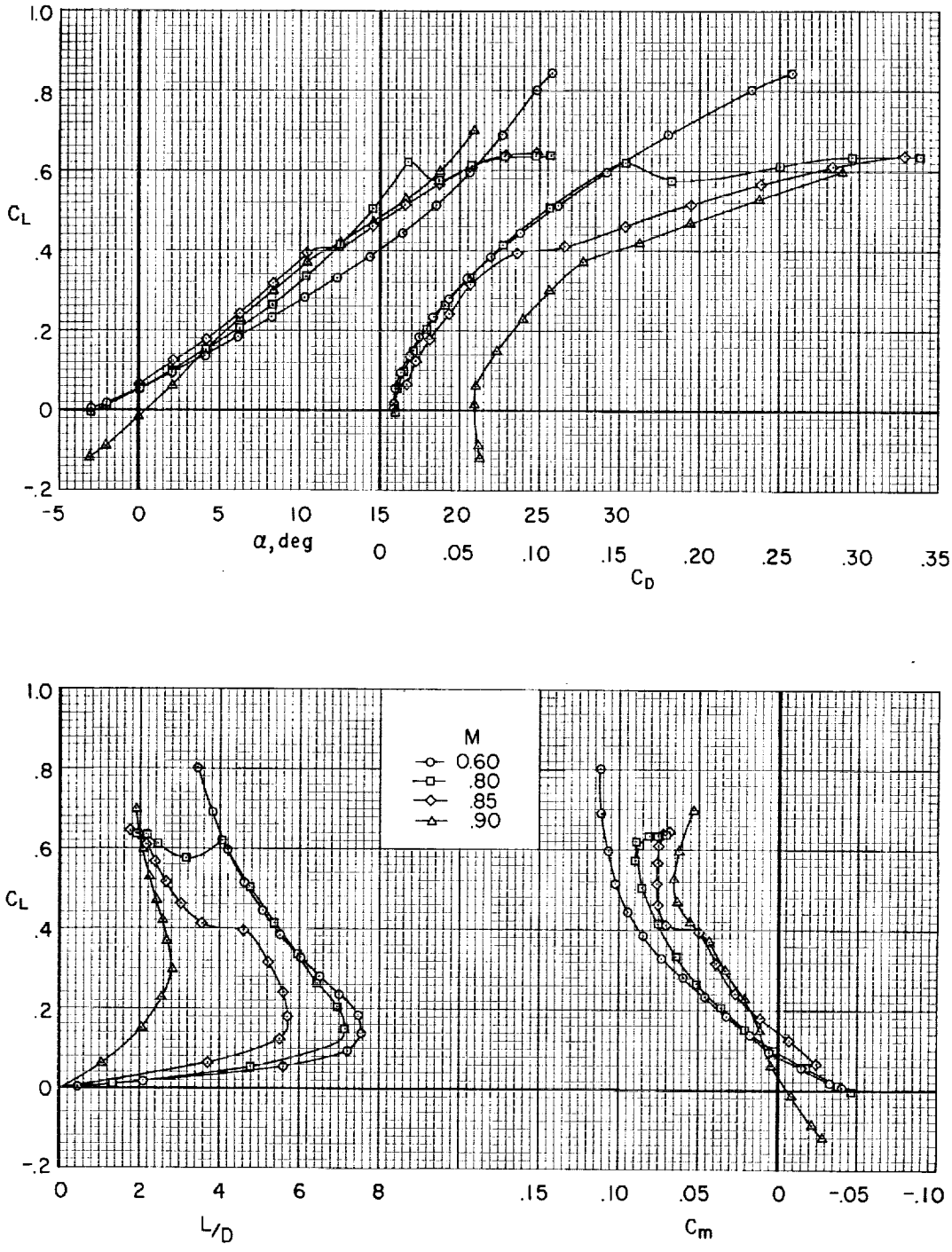

(a) t/d = 0.225, positive camber.

Figure 3.- The longitudinal aerodynamic characteristics of the models at several Mach numbers; R = 3.3×10^6.

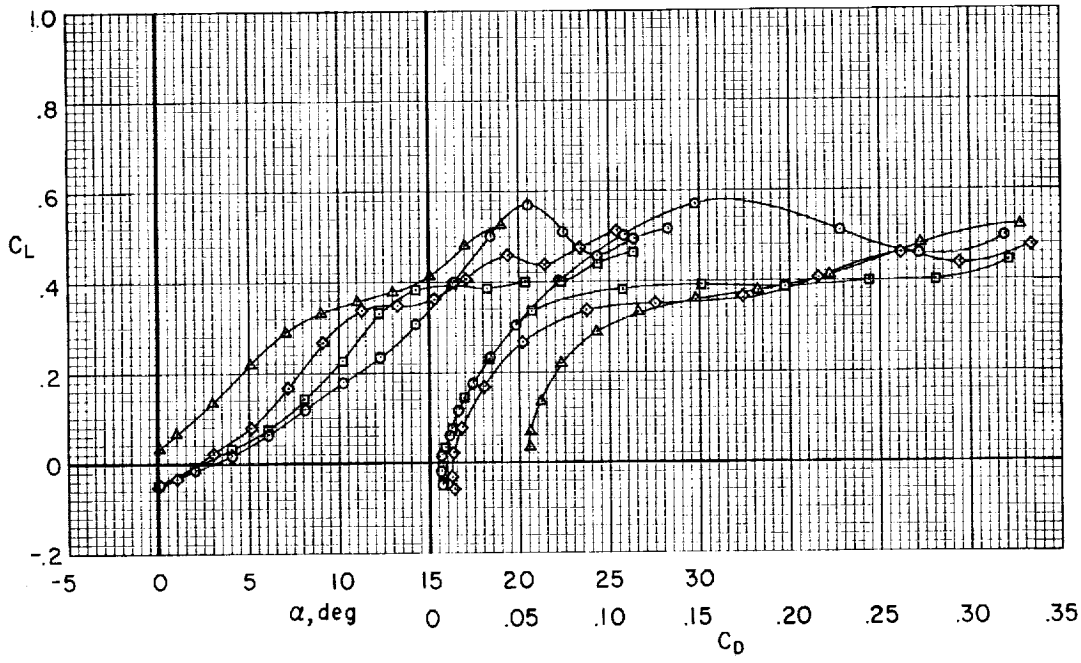

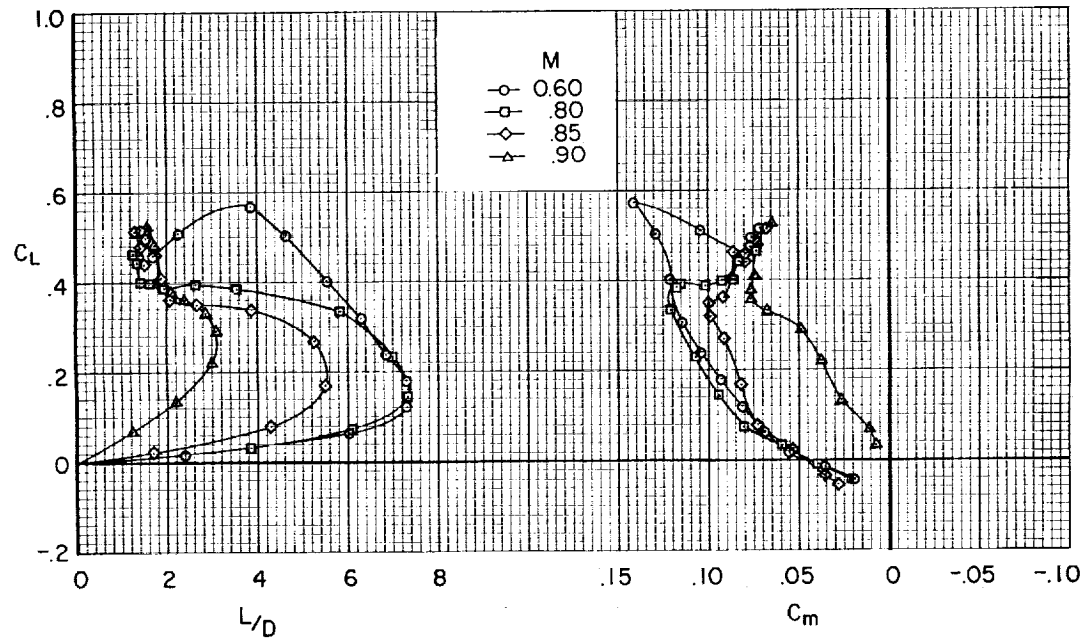

(b) t/d = 0.225, negative camber.

Figure 3.- Continued.

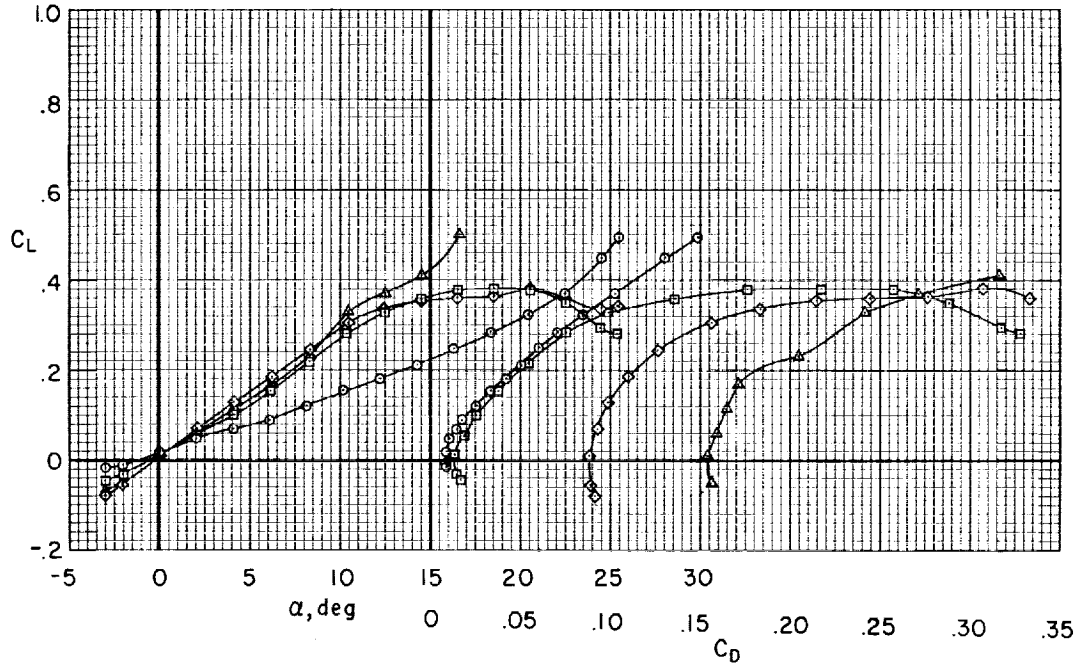

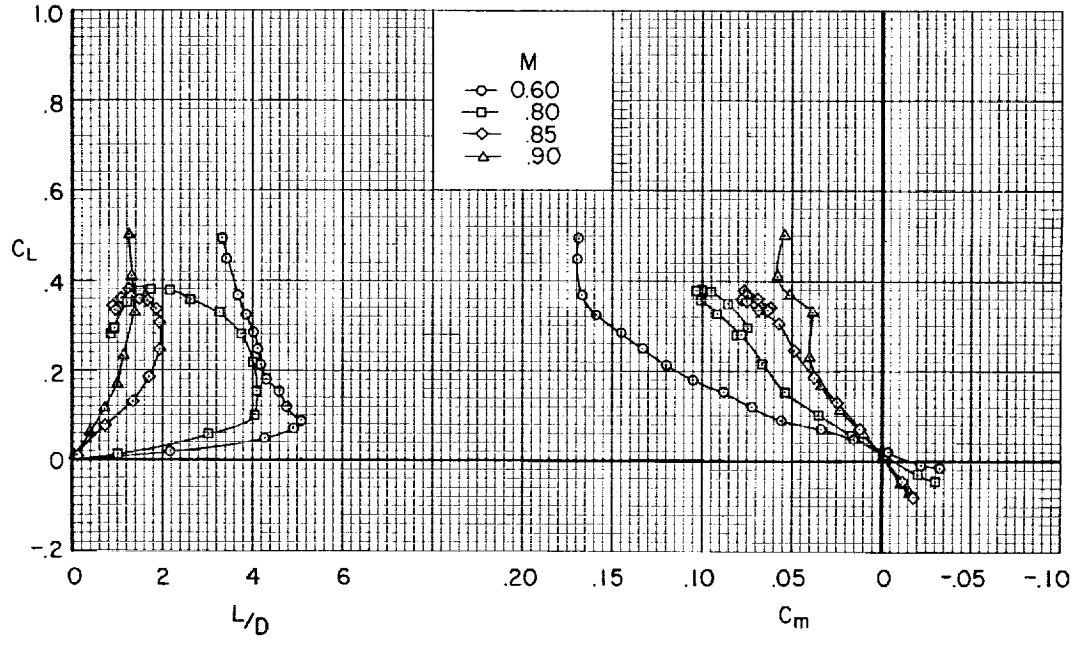

(c) t/d = 0.325

Figure 3.- Continued.

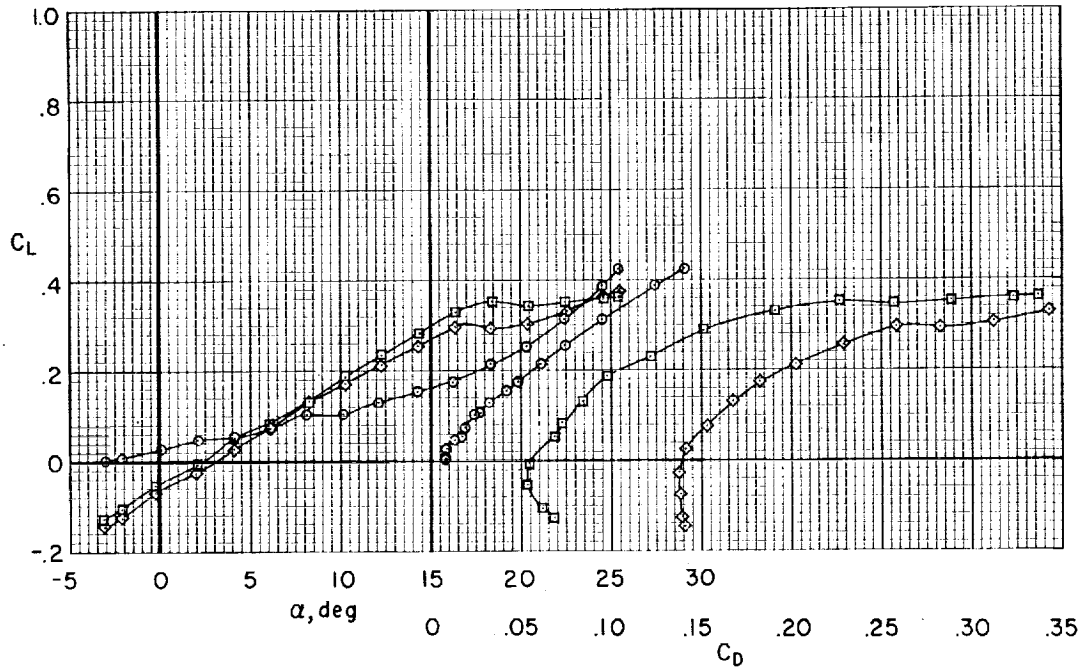

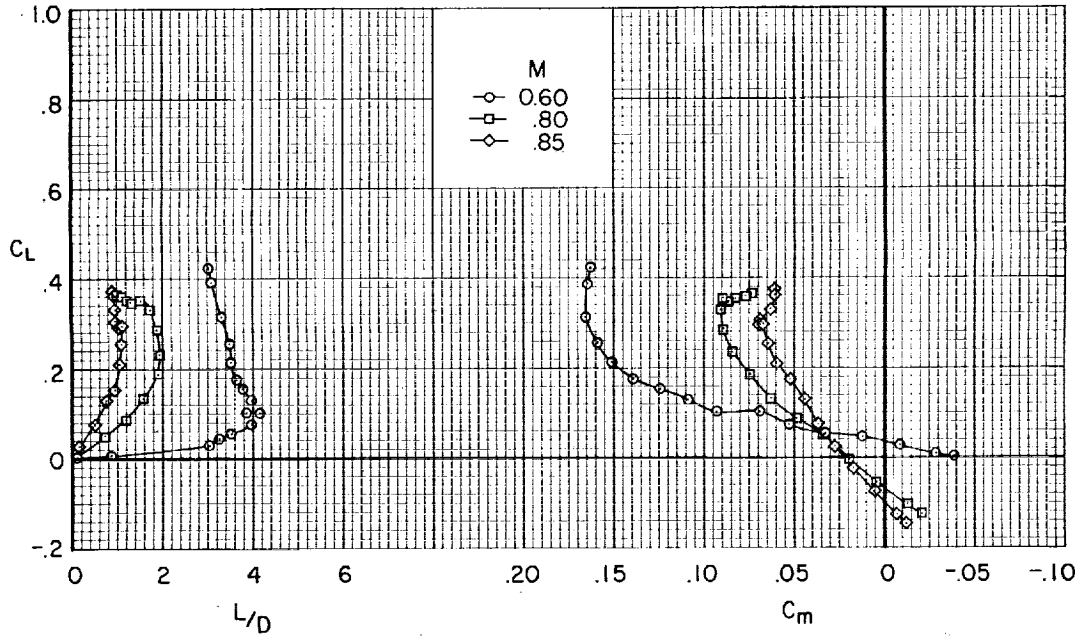

(d) t/d = 0.375, positive camber.

Figure 3.- Continued.

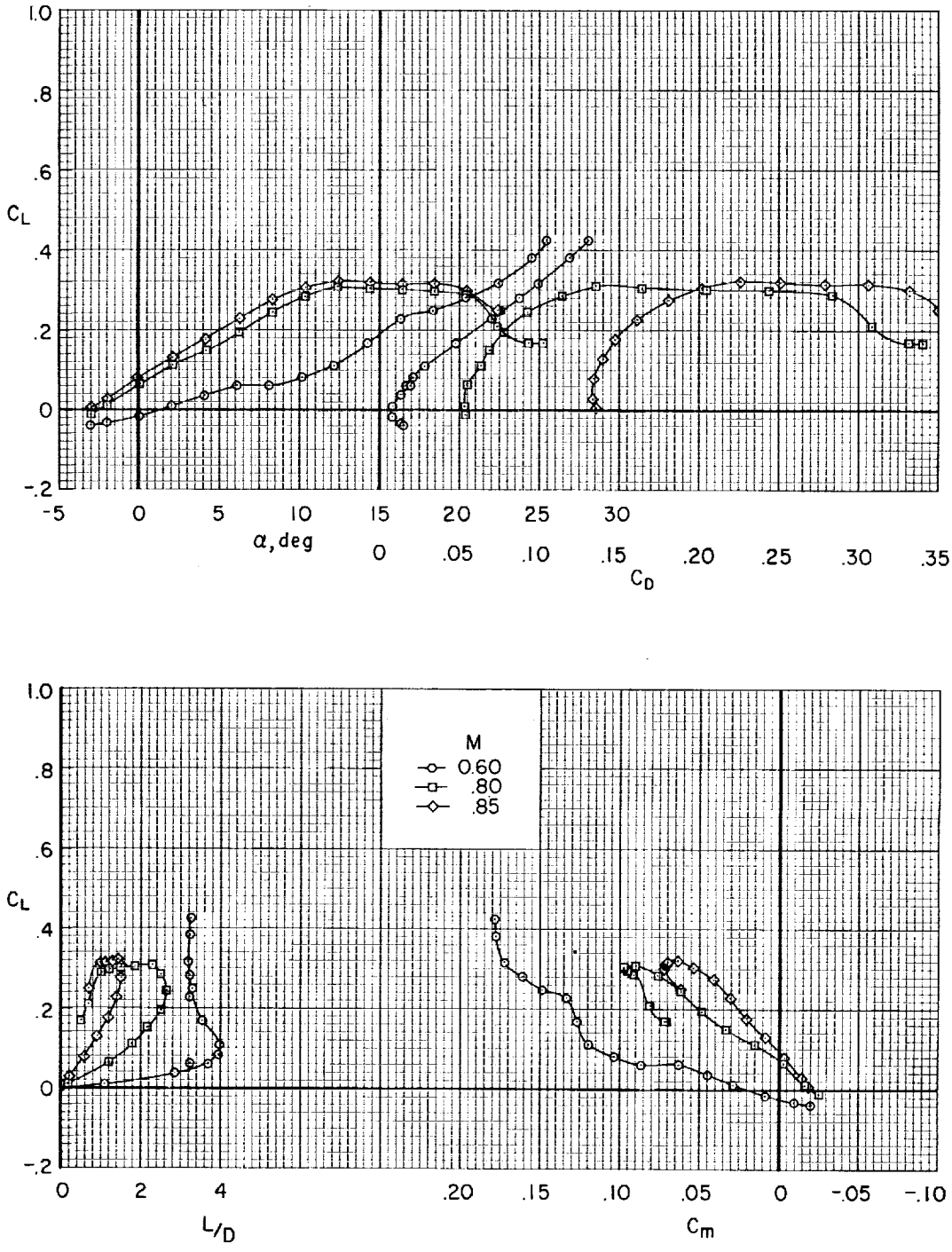

(e) t/d = 0.375, negative camber.

Figure 3.- Continued.

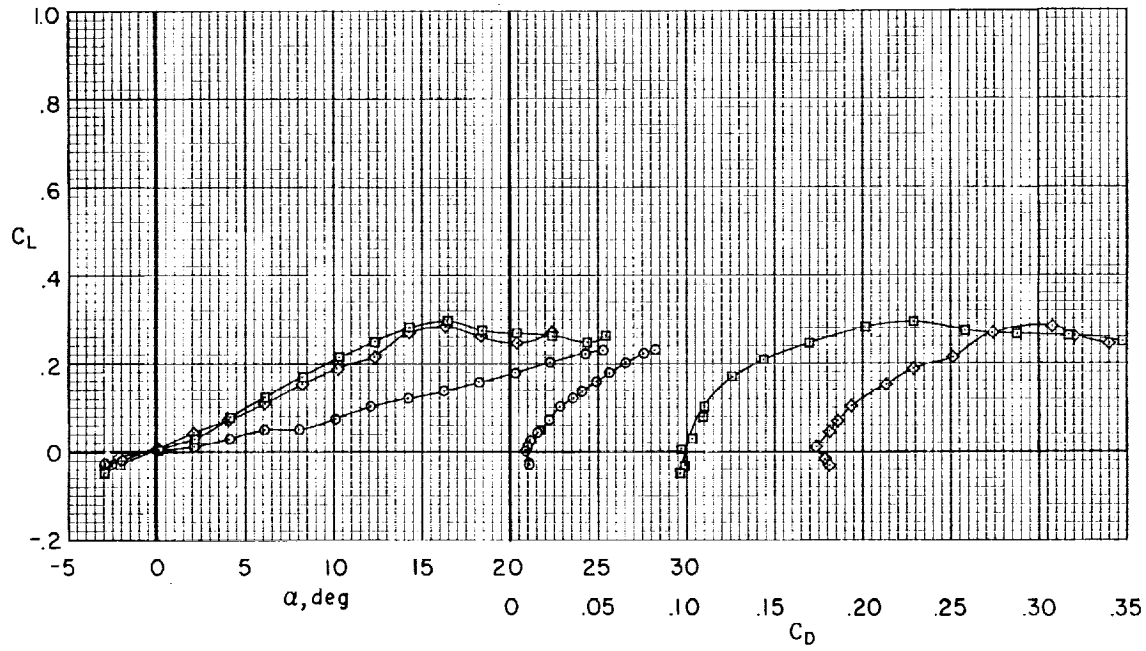

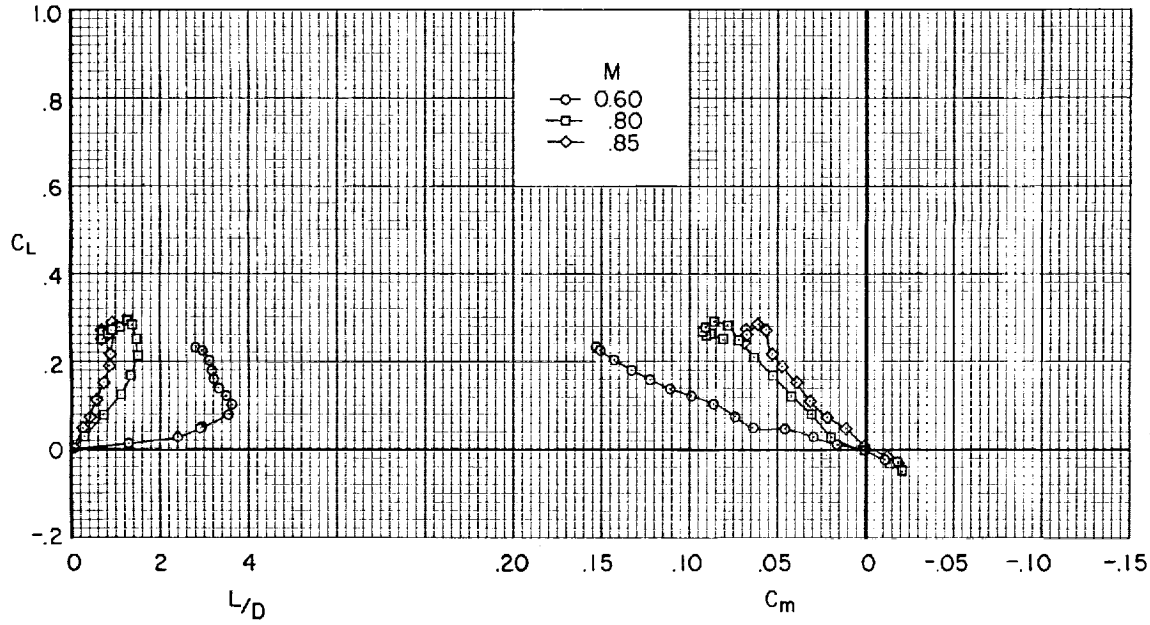

(f) t/d = 0.425

Figure 3.- Concluded

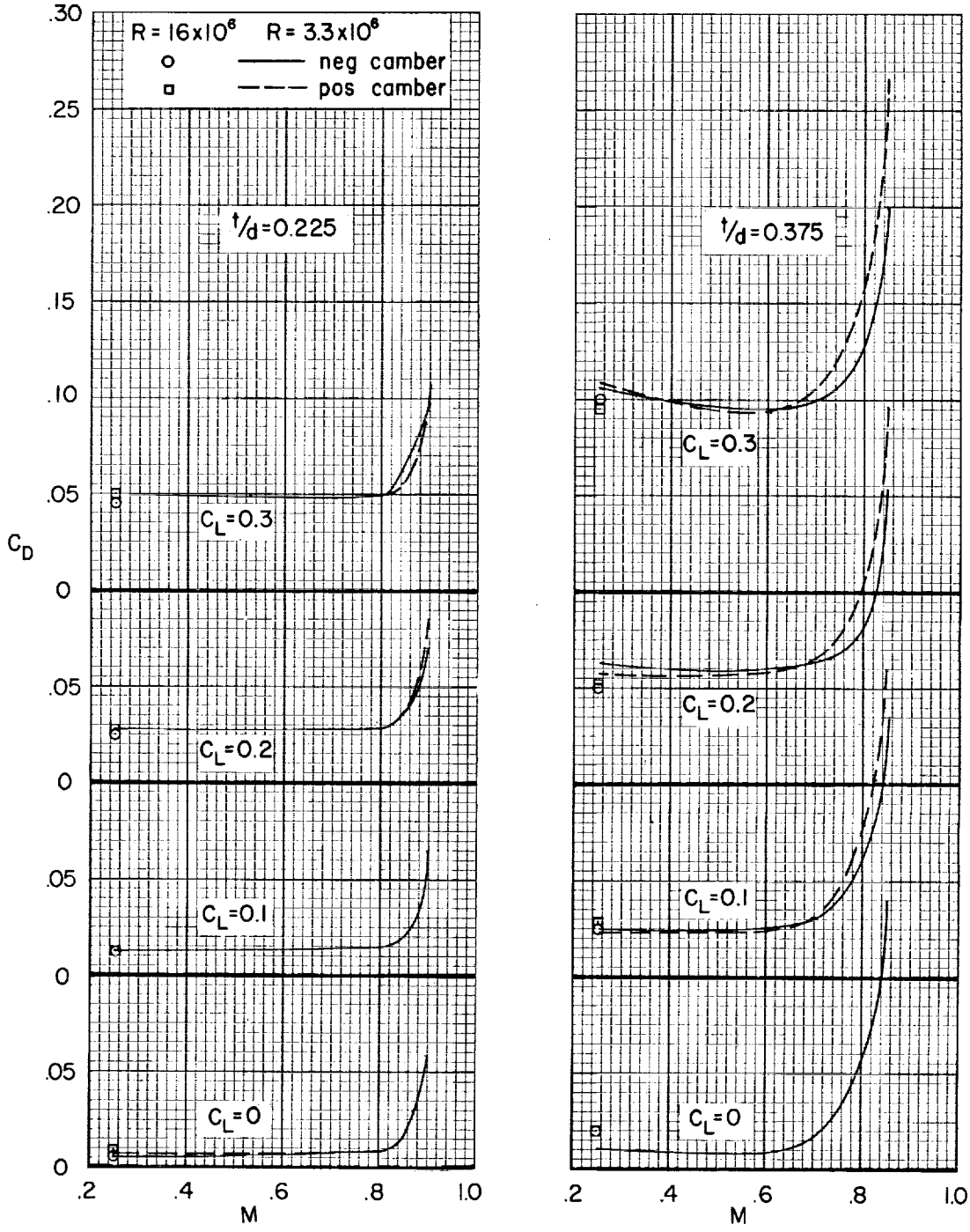

Figure 4.- The variation with Mach number of drag coefficient at constant lift coefficient for models having positive and negative camber.

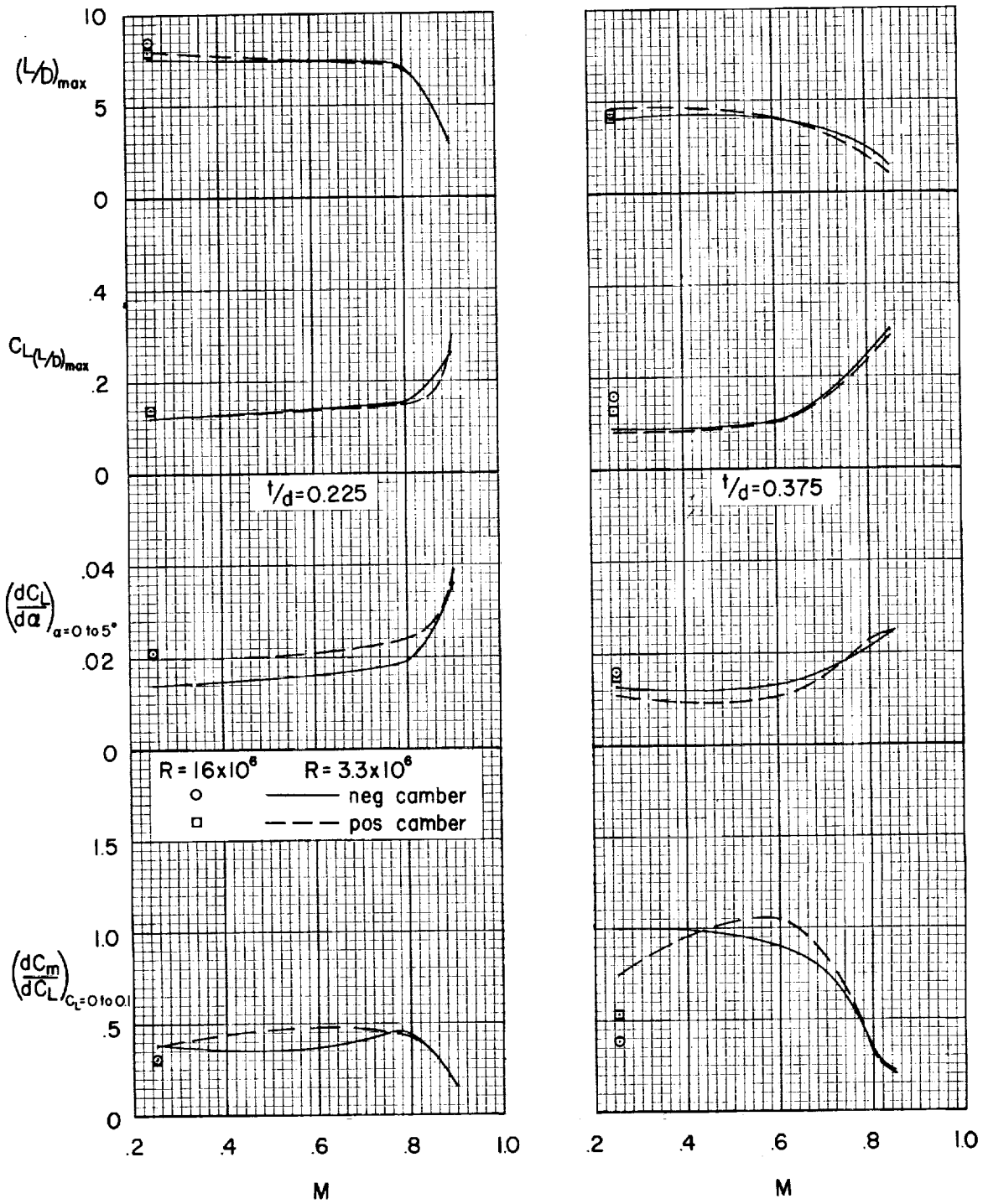

Figure 5.- The variation with Mach number of maximum lift-drag ratio and corresponding lift coefficient, and lift- and pitching-moment curve slopes for models with positive and negative camber.

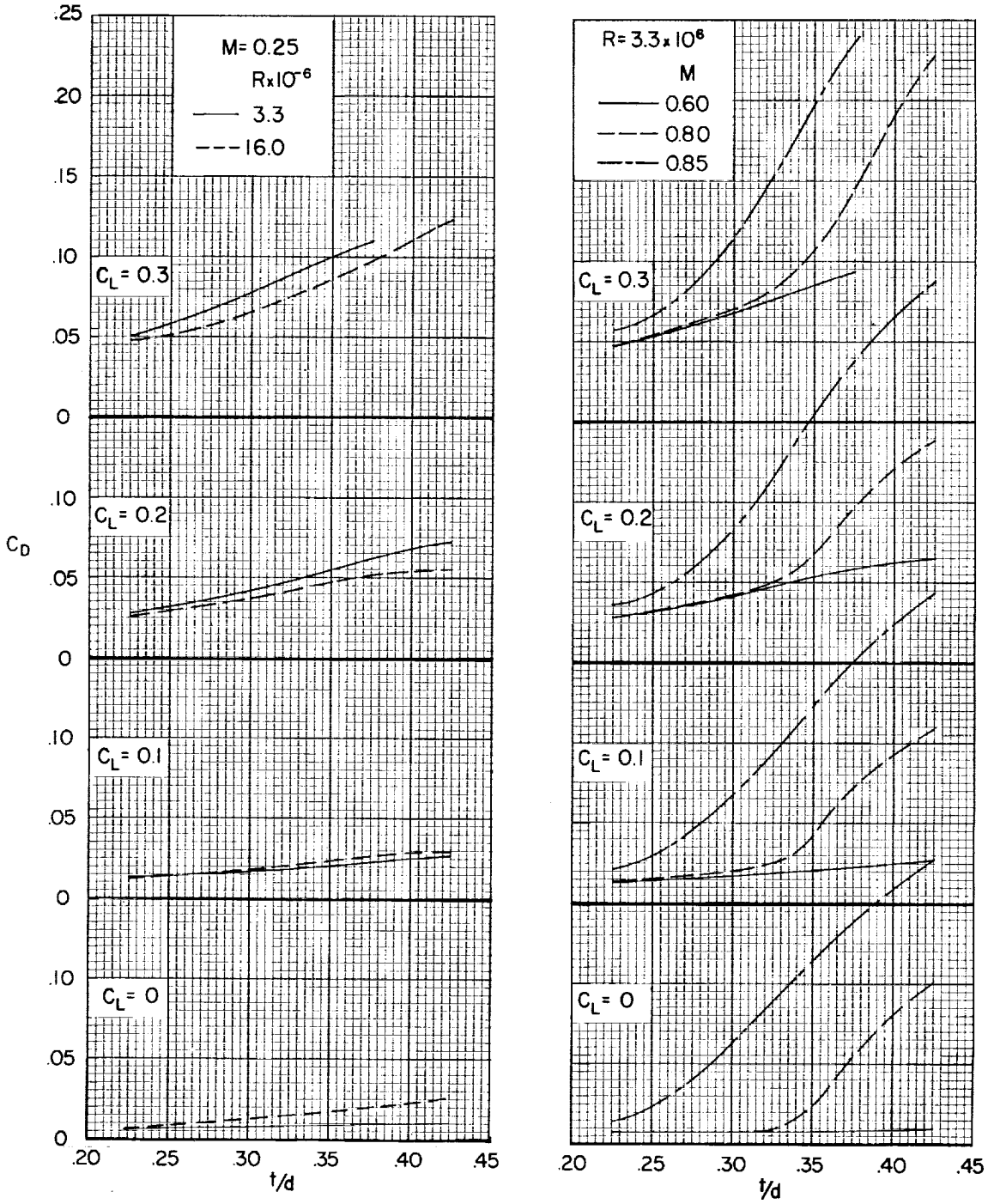

Figure 6.- The variation with thickness-diameter ratio of drag coefficient at constant lift coefficient.

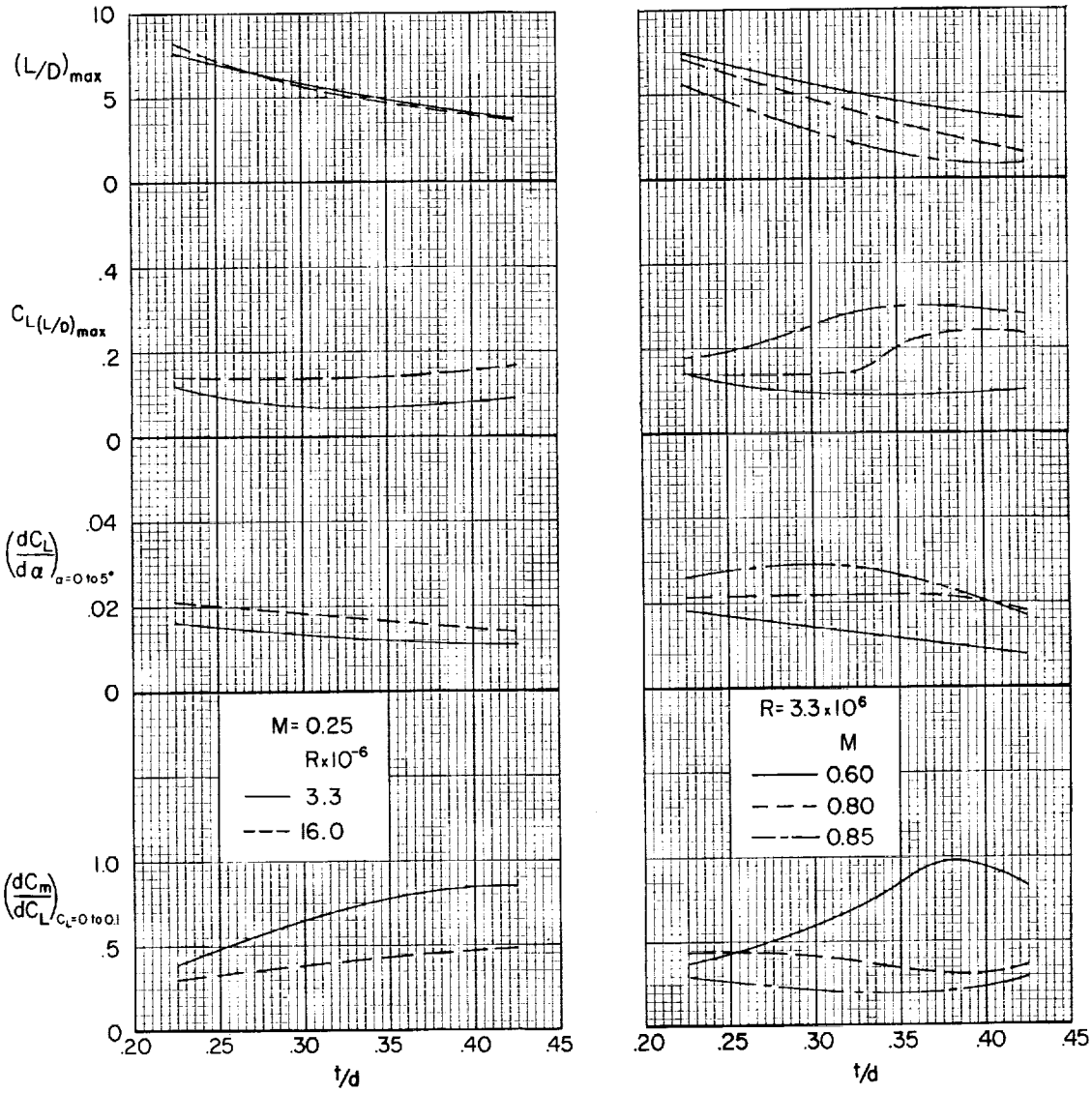

Figure 7.- The variation with thickness-diameter ratio of maximum lift-drag ratio and corresponding lift coefficient, and lift- and pitching-moment curve slopes.